Long-Wavelength InGaAsP/InP Multiquantum Well Distributed Feedback and Distributed Bragg Reflector Lasers Grown by Chemical Beam Epitaxy

W. T. Tsang, *Fellow, IEEE*, M. C. Wu, Y. K. Chen, F. S. Choa, *Member, IEEE*, R. A. Logan, *Fellow, IEEE*, S. N. G. Chu, A. M. Sergent, P. Magill, K. C. Reichmann, and C. A. Burrus, *Fellow, IEEE*

Abstract—We demonstrated the successful operation of long-wavelength InGaAsP low threshold-current index-coupled and gain-coupled DFB lasers grown by chemical beam epitaxy (CBE). For index-coupled DFB lasers, buried-heterostructure six-QW DFB lasers (250 μm long and as-cleaved) operated at 1.55 μm with CW threshold currents 10–15 mA and slope efficiencies up to 0.35 mW/mA (both facets). A side-mode suppression ratio (SMSR) as high as 49 dB was obtained. The lasers operated in the same range even at high temperatures (70 °C checked). For gain-coupled DFB lasers, gain-coupling is accomplished by using a InGaAsP quaternary grating or quantum-well grating that absorbs the DFB emission. The use of a quantum-well grating, in particular, greatly facilitates the reproducible regrowth (defect-free) over grating and the control of the coupling coefficient. CW threshold currents were in the range of 10–15 mA for 250-μm and 13–18 mA for 250-μm and 500-μm cavities, respectively. Slope efficiencies were high, ~0.4 mW/mA (both facets). SMSR was as high as 52 dB and remained in the same DFB mode with SMSR staying ~50 dB throughout the entire current range. Linewidth × power products of 1.9–4.0 were measured with minimum linewidths of 1.8–2.2 MHz. No detectable chirp was measured under 2.5 Gb/s modulation. Unlike index-coupled DFB lasers in which mode partition events decrease slowly even when biased above threshold, these lasers have mode partition events shut off sharply as bias approaches threshold ($\gtrsim$0.95 I_{th}). A very small dispersion penalty of 1.0 dB was measured at 10^{-11} BER in transmission experiments using these lasers as sources at 1.7 Gb/s over an amplified fiber system of 230 km. No self-pulsation was observed in these gain-coupled DFB lasers. Gain-switching at 4 GHz with a 100% optical modulation depth and a FWHM pulse width of 23 ps was achieved with these gain-coupled DFB lasers. The peak power was ~72 mW and the FWHM bandwidth was 0.14 nm. We also fabricated InGaAs/InGaAsP multiquantum-well DBR lasers by CBE. Taking advantage of uniform thickness growth and proper design of weak and long gratings, a record high SMSR of 58.5 dB was obtained.

I. INTRODUCTION

MULTIQUANTUM-WELL (MQW) distributed feedback (DFB) lasers in the 1.3–1.55 μm wavelength range employing the InGaAsP/InP materials have been investigated very intensively [1]. This is because they offer very impor-

tant performance advantages over bulk-active DFB lasers, such as reduced frequency chirping under high-speed direct modulation, narrower linewidth, larger TE/TM mode discrimination, and lower threshold currents, etc. To date, metalorganic vapor phase epitaxy (MOVPE) is almost the exclusive epitaxial growth technique employed in their preparation [2], [3]. Liquid-phase epitaxy is incapable of growing the thin layer structures needed for the MQW lasers. Similarly, the fast growth rate of the hydride VPE tends to render the growth of the MQW thin layers not easily controllable due to the short growth times needed. Recently, we have demonstrated that chemical beam epitaxy (CBE) [4] is capable of growing 1.5-μm wavelength strained-layer graded-index separate-confinement heterostructure (GRINSCH)QW lasers [5] having extremely low threshold current density of 170 A/cm^2, internal quantum efficiency of 83%, and internal waveguide loss of 3.8 cm^{-1}. However, the preparation by CBE of DFB lasers remains a great challenge and of technological importance because *defect-free* growth over corrugated surface (grating) proves to be a nontrivial process even for MOVPE. Technologically, CBE is well suited for the growth of DFB laser wafers because of its high degree of precise thickness and composition control, and large-area uniformity. Such control and uniformity are essential in producing DFB lasers with uniform device performance such as lasing wavelength and optical coupling.

In this paper, we demonstrate the successful growth of 1.5-μm wavelength strained-layer InGaAs/InGaAsP MQW DFB lasers by CBE and review the device performance. In particular, we also report a gain-coupled DFB laser with a new grating structure using quantum-well layers, and a distributed bragg reflector (DBR) laser with a record high side-mode suppression ratio (SMSR) of 58.5 dB.

II. INDEX-COUPLED DFB LASERS

In this DFB structure, InGaAsP quaternary grating (bandgap wavelength $\lambda = 1.25$; for convenience it will be referred to as $Q_{1.25}$) is placed at the bottom of the MQW stack with an InP spacer layer.

Figure 1(a) shows a schematic diagram of the laser structure together with a cross-section TEM photograph in Fig. 1(b). To fabricate this, a uniform n-type $Q_{1.25}$ layer of the desired thickness (in this sample, 62 nm was used) for grating
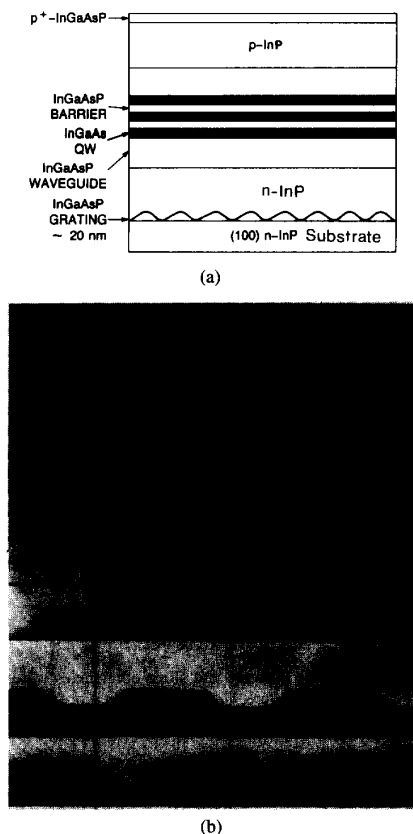
(a)

(b)

Fig. 1.   (a) A schematic diagram of the MQW DFB laser structure with a bottom quaternary grating. (b) A cross-sectional TEM photograph ([200] dark field) of a CBE-grown strained-layer 6-QW DFB laser wafer. Defect-free InP over-growth was achieved with no grating erosion.

fabrication was grown over a 2-inch-diameter (100)-oriented n-InP substrate. It has been shown previously that the present CBE system is capable of producing layers having a thickness uniformity of $\lesssim \pm 1\%$ and a photoluminescence (PL) peak wavelength uniformity of $\lesssim \pm 5$ nm (as good as ± 1.5 nm) [6], [7]. Recent results from other research groups also obtained thickness variations $\leq 0.75\%$ and bandgap wavelength variations of InGaAsP quaternaries $\lesssim \pm 1$ nm over 3-inch-diameter wafers with CBE [8]. First-order gratings were prepared by standard holographic techniques and wet etching and had an amplitude of ~ 22 nm as shown in Fig. 1(b). In this sample, the etched grating depth is not deep enough to penetrate the entire thickness of the $Q_{1.25}$ layer. 22 nm was used to reduce the coupling coefficient. By growing the appropriate $Q_{1.25}$ thickness and controlling the etching times, quaternary gratings completely buried in InP material can be obtained. At the same time, the depth of the grating is automatically given by the thickness of the $Q_{1.25}$ layer. After cleaning, the sample was reintroduced into the CBE system for MQW laser regrowth. The substrate was heated up to $\sim 545°$ C under phosphorus overpressure from precracked phosphine (PH_3). Under such low-temperature conditions, no grating erosion was ever observed. The detailed shape of the grating was well preserved, as shown by the TEM photograph in Fig. 1(b). An

n-type InP spacer layer of the desired thickness (68 nm in the present laser) for controlling the coupling constant κ was grown. This was then followed by a standard strained-layer six-QW separate-confinement heterostructure. The strained-layer $In_xGa_{1-x}As$ QW's ($x \sim 0.65$) and $Q_{1.25}$ barriers were 4.8 and 25 nm, respectively. The $Q_{1.25}$ waveguide layer on each side of the MQW stack was 75 nm. The structure was grown with all-vapor sources, including the n- and p-type dopings. Diethylzinc and tetraethyltin or hydrogen sulphide were used as the p-type and n-type doping sources, respectively. Finally, buried-heterostructure lasers were formed by MOVPE regrowth with semi-insulating iron-doped InP. In MOVPE regrowth over grating, especially over InP gratings on the substrate surface, extreme care is needed in order to avoid serious grating erosion [2] during the substrate heat up to ~ 630 °C. On the other hand, it was found that a controlled amount of mass transport is needed for the successful growth of dislocation-free epilayer structure over the gratings. Since the exact amount of mass transport is rather difficult to control reproducibly, the resulting grating shape and depth can affect the coupling constant κ in an unpredictable manner. Yet, it has been shown that the device characteristics, e.g., spectral linewidths, harmonic distortions, and relative intensity noise, etc., depend sensitively on the coupling constant [9]. An examination of the CBE-grown DFB wafers using TEM shows no mass transport of the quaternary grating profile. More importantly, no dislocation defects were observed, and the QW multilayers were extremely flat. An example is shown by the TEM photograph in Fig. 1(b). We have found that unlike MBE, CBE is more similar to MOCVD. The growth of InP over corrugated surface has a smoothing effect though not as strong as MOCVD. This is expected from the longer diffusion lengths of the surface metalorganic species.

In the case of the InP substrate grating $Q_{1.1}$ is usually grown first. This is dictated by the waveguide design requirement and the greater tolerance in lattice matching of $Q_{1.1}$, as it is relatively close to the InP material. As a consequence, the refractive-index difference between the InP grating and the $Q_{1.1}$ overlayer is small. There is no such limitation when quaternary grating is employed. Further, the growth of quaternary over corrugated surface exposing different crystal planes may result in locally mismatched and nonuniform materials. Severe cases lead to the generation of dislocation defects. This may explain why mass transport is needed for dislocation-free growth of quaternaries over InP gratings. On the other hand, there is no such issue when InP is grown over quaternary gratings, and InP smooths out the corrugation much faster than quaternary overlayers [see Fig. 1(b)].

The resulting DFB lasers [10] (250-μm-long cavity and both facets as-cleaved) operated at 1.55 μm with CW threshold currents 10–15 mA and slope efficiencies up to 0.35 mW/mA (both facets). Side-mode suppression ratios (SMSR) as high as 49 dB have been obtained in as-cleaved lasers without facet coatings. These performance values are among the best DFB lasers grown by other techniques [1], [2]. Typical light–current (L–I) and current–voltage characteristics are shown in Fig. 2. The inset shows the spectrum obtained at output power of ~ 15 mW/facet. A SMSR of 48.5 dB was obtained. The laser
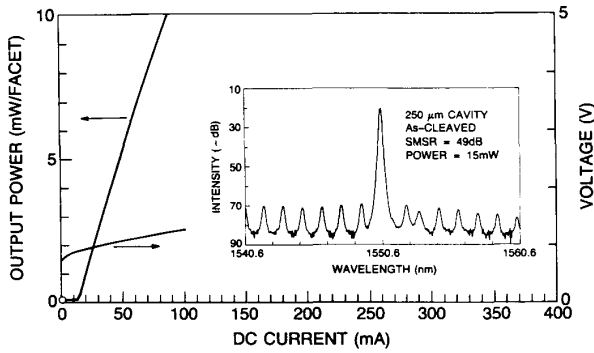
Fig. 2. The light–current and current–voltage characteristics of a typical CBE-grown buried heterostructure MQW DFB laser. The inset shows the spectrum obtained at an output power of ∼15 mW/facet. A SMSR of 48.5 dB was measured.
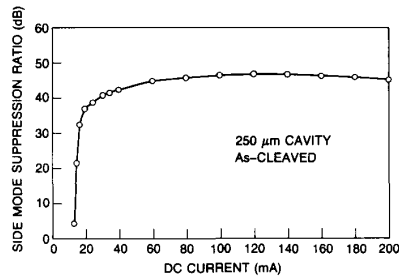

Fig. 3. The SMSR as a function of injection current.
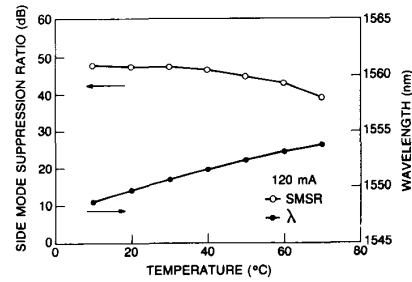

Fig. 4. The SMSR and lasing wavelength were measured as a function of temperature, keeping the operating current constant at 120 mA.

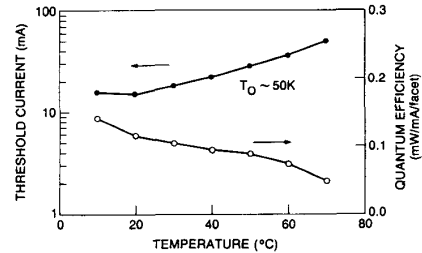Fig. 5. The CW threshold currents and slope efficiencies were plotted as a function of heat-sink temperature.

operated in the same DFB mode, with SMSR staying above 40 dB starting right above threshold and throughout the entire current range, as shown in Fig. 3. No mode jumps were observed in the threshold crossing. We also investigated the device performance as a function of heat-sink temperature. Keeping the operating current constant, the SMSR and lasing wavelength were measured as a function of temperature. The DFB laser stayed stably in the same DFB mode and with high SMSR even at high temperatures (70 °C checked here) with the operating current maintained at 120 mA. As shown in Fig. 4 SMSR decreased from 48 dB at 10 °C to 40 dB at 70 °C, while the lasing wavelength increased at a rate of 0.083 nm/°C. In Fig. 5 we show the CW threshold currents and slope efficiencies as a function of temperature. The threshold temperature-dependence coefficient T_0 is ∼50 K. In DFB lasers T_0 is somewhat meaningless because it depends on the relative detuning of the DFB mode with respect to the gain peak. For actual system applications, antireflection/high-reflection (AR/HR) coatings are needed in order to increase the slope efficiency and the output power from the output facet. It will also increase the high-temperature operation range of the diode.

III. GAIN-COUPLED DFB LASERS WITH QUATERNARY GRATINGS

The oscillation wavelength degeneracy at the edges of the Bragg reflection band is a major problem in index-coupled DFB [11]–[15] lasers. One solution to this problem

is the use of AR/HR-coated facets. This, however, causes a yield problem associated with the uncertainty of the facet phases [11]. Another solution is the incorporation of a $\lambda/4$ or corrugation-pitch modulated phase shift [12], [13], [16]. For perfect AR coatings, these lasers show a high yield, while deteriorating rapidly for reflectivities of only a few percent [12]. Other drawbacks include the wasting of practically half of the power from the back facet, and high spatial hole burning caused by the $\lambda/4$ phase shift [13] (this is reduced by the corrugation-pitch modulation scheme [16]). The high spatial hole burning gives rise to optical nonlinearity in the light–current curves, increased spectral linewidth, and a less flat frequency-modulation response.

An alternative approach is the introduction of gain coupling [15], [17], [18]. Purely gain-coupled lasers theoretically should have one lasing mode exactly at the Bragg wavelength for AR-coated facets, thereby solving the degeneracy problem [15]. It is shown theoretically [19], [20] that even a small degree of gain coupling enhances the performance considerably in terms of threshold gain difference (side-mode suppression ratio) and removes the degeneracy of an AR-coated DFB laser. Moreover, a complete elimination of spatial hole burning is possible [20]. This in turn will further increase the laser yield. For non-AR-coated lasers, it is shown [21], [22] that there s a relevant improvement in yield even for a small amount of gain coupling. In addition, results also show a potential for lower feedback sensitivity compared to other DFB lasers [23]. The validity of the gain-coupled approach for semiconductor DFB lasers has been demonstrated recently in GaAs/AlGaAs lasers [17], [18]. Very recently, 1.5-μm gain-coupled DFB lasers were also demonstrated using varying active layer thickness [24] and in AlGaInAs systems [25]. In this experiment, we
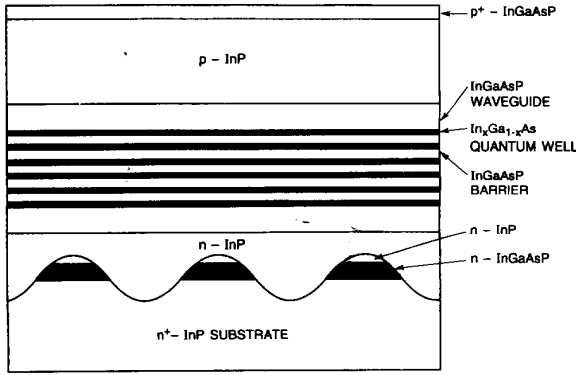
Fig. 6. A schematic diagram of the MQW DFB laser structure with a bottom buried loss-coupled quaternary grating.
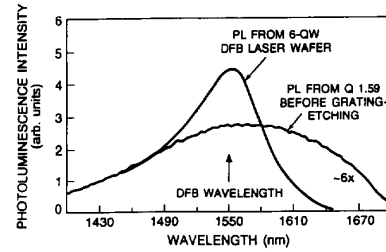

Fig. 7. The photoluminescence spectra from the grating $Q_{1.56}$ measured before grating-etching, and the 6-QW $In_{0.6}Ga_{0.4}As/Q_{1.25}$ active-layer DFB laser wafer after regrowth over the $Q_{1.56}$ grating.

demonstrate the use of loss-coupled (since the resultant effect is a periodic gain modulation, we will refer in the following as gain-coupled in accordance with the convention) InGaAsP quaternary grating and InGaAs/Inp quantum-well grating for long-wavelength DFB lasers. The amount of gain-coupling coefficient κ_g is controlled by the composition (bandgap) or thickness of the quaternary or InGaAs quantum-well grating chosen.

In Fig. 6 we show schematically the proposed DFB laser structure. As an illustrative example, a 1.5-μm In-GaAs/InGaAsP with a InGaAsP quaternary grating is shown. The grating grooves have etched through the InGaAsP layer to form isolated InGaAsP grating lines buried in InP. This yields the largest possible gain modulation since the burying InP is lossless. To fabricate this, a uniform layer of 20-nm n-type $Q_{1.56}$ was grown on a 2-inch-diameter (100)-oriented n-InP substrate capped by a 5-nm InP top layer. This ensures that there is optical absorption at the lasing wavelength, 1.55 μm. First-order gratings were prepared by standard holographic techniques and wet etching, and had an amplitude of ~50 nm. No precise grating depth control was exercised here as long as the $Q_{1.56}$ epilayer was completely etched through. After cleaning, the sample was reintroduced into the CBE system for MQW laser regrowth. An n-type InP spacer layer of the desired thickness (65 nm in the present laser) was grown. The thickness of this layer will also affect the value of both the index- and the gain-coupled coefficients. Because the $Q_{1.56}$ is thin and the top surface is capped with InP layer, subsequent regrowth of InP over such a grating is essentially the same as growing InP on InP. This makes regrowth over grating a trivial task and guarantees a defect-free structure as examined by TEM. This was then followed by the standard strained-layer 6-QW separate confinement heterostructure (SCH) [26], [27]. The quaternary, $Q_{1.25}$, waveguide layers were 52.2 nm each. The strained-layer $In_{0.6}Ga_{0.4}As$ QW's and $Q_{1.25}$ barriers were 5 nm and 18.6 nm, respectively. These laser wafers were further processed into buried heterostructure employing MOVPE regrowth of Fe-doped InP at 630 °C.

In Fig. 7 we show the photoluminescence (PL) spectrum of the grating $Q_{1.56}$ measured before grating-etching together with the PL spectrum from the 6-QW $In_{0.6}Ga_{0.4}As(5$

nm)/$Q_{1.25}$(18.6 nm) active-layer DFB laser wafer after regrowth over the $Q_{1.56}$ grating. It is seen that optical absorption has extended well beyond 1550 nm. This suggests that the present $Q_{1.56}$ grating will produce a gain-coupled component in addition to the index-coupled component due to index of refraction difference between InP and $Q_{1.56}$. It is important to point out that this index refraction difference increases as the quaternary bandgap decreases. Thus, thinner quaternary layer is needed for the same index refraction difference. This facilitates the regrowth over the grating.

The resulting DFB lasers (250-μm-long cavity and both facets as-cleaved) operated at 1.55 μm with CW threshold currents 10–15 mA and slope efficiencies up to 0.4 mW/mA (both facets). Such performance is similar to that of the index-coupled DFB lasers described above. This indicates that with optimally designed gain-coupled DFB lasers, the presence of the loss-coupled grating did not noticeably increase the threshold currents and decrease the slope efficiencies. Theoretically, it is expected that even a small degree of loss coupling will enhance the performance considerably. Hence, in our present design, we have an estimated loss coupling coefficient $\kappa_g \sim 4\,cm^{-1}$. Such small additional loss is not expected to increase the threshold currents or decrease the slope efficiency noticeably. Side-mode suppression ratios as high as 52 dB have been obtained in as-cleaved lasers without facet coatings. In fact, these performance values are among the best DFB lasers. A typical light–current characteristic is shown in Fig. 8. The inset shows the spectrum obtained at output power of ~20 mW/facet. A very large SMSR of 52 dB was obtained. The laser operated in the same DFB mode with SMSR above 45 dB starting above threshold and stayed at ~50 dB throughout the entire current range, as shown in Fig. 9. No mode jumps were observed in the threshold crossing, in contrast to a similar structure but with purely index-coupled DFB lasers [28]. It is important to point out that of the seven lasers CW-bonded for checking the spectra, all have the same single DFB mode (the longer wavelength one).

Since the $Q_{1.56}$ grating segments have a higher refractive index and are optically absorbing, the Bragg mode, which has its standing-wave peaks aligned with these $Q_{1.56}$ segments, will suffer more loss and has a shorter wavelength ($\lambda = c/\nu n$, where c is the speed of light, ν the frequency, and n the index of refraction) than the other Bragg mode, which aligns with the InP troughs of the grating. This explanation is not perfect, but seems to be consistent with our experimental observation.
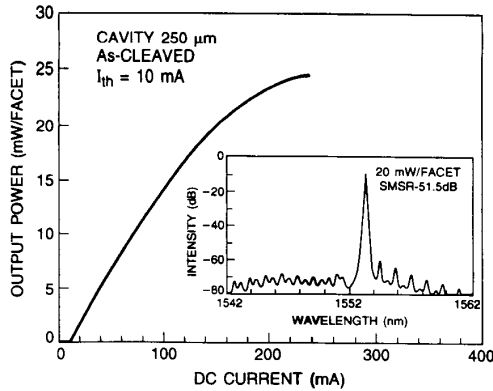
Fig. 8. The light–current characteristic of a typical as-cleaved CBE-grown buried-heterostructure gain-coupled MQW DFB laser. The inset shows the spectrum obtained at an output power of ∼20 mW/facet. A SMSR of 52 dB ws measured.
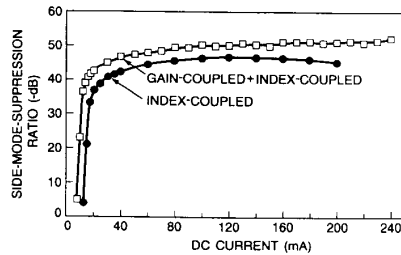

Fig. 9. The SMSR as a function of injection current for a 1.5 μm wavelength gain-coupled and an index-coupled DFB laser.
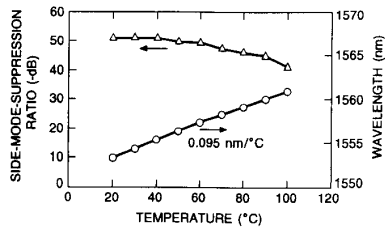

Fig. 10. The side-mode-suppression ratio and lasing wavelength for a gain-coupled DFB laser as a function of heat-sink temperature.

Although this result is rather preliminary, it appears to agree with the theoretical expectation that even a small degree of gain coupling enhances the performance considerably in terms of threshold gain difference, and removes the degeneracy. Our estimated κ_g is ∼4 cm^{-1} using an absorption loss of ∼2 · 10^4 cm^{-1} for Q$_{1.56}$. The κ_i is less than ≲50 cm^{-1}. No self-pulsation was observed.

We also investigated the device performance as a function of heat-sink temperature. Keeping the operating current constant, the SMSR and lasing wavelength were measured as functions of temperature. The DFB laser stayed stably in the same DFB mode and with high SMSR even at high temperatures (100 °C checked here). Fig. 10 shows an example with the operating current maintained at 160 mA. SMSR decreased from 52 dB at 20 °C to 41 dB at 100 °C, while the lasing wavelength increased at a rate of 0.095 nm/°C. The threshold-temperature

dependence coefficient T_0 is ∼80 K between 20 and 40°C. At 100 °C, the CW threshold current is still very low, 50 mA. As measured previously, the temperature behavior of DFB lasers depends on the relative position of the DFB mode with respect to the gain peak. A detailed discussion can be found in [28]. For actual system applications, antireflection/high-reflection (AR/HR) coatings are needed in order to increase the slope efficiency and the output power from the output facet. It will also improve the high-temperature operation of the diode.

IV. GAIN-COUPLED DFB LASERS WITH QUANTUM- WELL GRATINGS

To investigate gain-coupled DFB lasers and achieve fine control of κ, we further propose a new grating layer structure using quantum wells. In Fig. 11 we show schematically the proposed DFB laser structure. As an illustrative example, a 1.5-μm In$_x$Ga$_{1-x}$As/InGaAsP multiquantum-well active-layer laser with a 2-QW In$_y$Ga$_{1-y}$As/InP grating is shown. The key innovation in this structure is the use of a QW structure for the grating. This offers great design flexibility and several important advantages. 1) Because the QW's are thin and interleaved with InP barriers, and the top surface is capped with an InP layer, subsequent regrowth of InP over such a grating is as mentioned earlier, essentially the same as growing InP on InP, making regrowth over grating a trivial task and guaranteeing a defect-free structure. 2) The coupling coefficient κ can be conveniently controlled by the number, the composition, or the thickness of the QW's. Further, the depth profile of the grating can be tailored by having QW's of different thicknesses or compositions or barriers. 3) Since the optimal coupling constant κL, where L is the laser cavity, should be approximately 1 to 2 for the best device performance, a relatively weak grating effect is sufficient. Thus, in practice, only very few QW's are needed. This allows all the QW's to be completely etched through during the grating formation (see the example in Fig. 12). As a result, the actual grating depth plays no role in affecting the κ. This significantly lessens the stringent requirement in grating depth control in conventional DFB laser structures. 4) Since the index of refraction of InGaAsP quaternary material increases as the bandgap of the material becomes narrower, by using narrower bandgap material for the grating quantum wells, the QW thickness can be further reduced. Furthermore, because of the quantum-size effect, the absorption edge of the QW grating can be designed to be above the lasing wavelength even if the same material composition as the active layer is used in the grating QW's. 5) On the other hand, if a gain- (loss)-coupled grating is desired, the thickness or composition of the grating QW's can be designed so that the absorption edge is below the lasing wavelength. If necessary, the grating QW's can have a composition with a narrower bulk bandgap than the active QW material. Figure 11 illustrates such possibilities with In$_x$Ga$_{1-x}$As/InGaAsP active QW's and an In$_y$Ga$_{1-y}$As/InP QW grating. In this example, x and y can be designed independently and varied over wide ranges. 6) The QW grating can also be composed of strained-layer material, either tensile or compressive. This may further
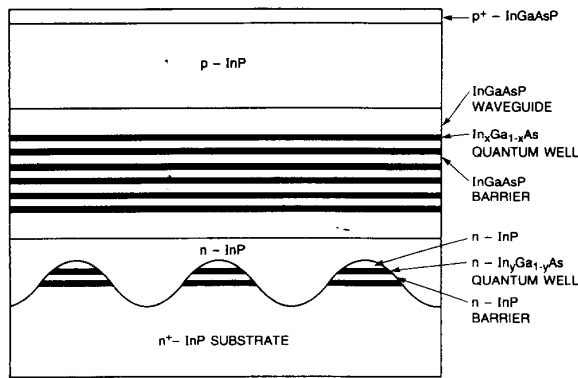
Fig. 11.   A schematic diagram of the MQW DFB laser structure with a bottom 2-QW grating.

Fig. 13.   The electroluminescence patterns along the laser stripe viewed through a contact window on the InP substrate when the DFB laser is biased below (a) and above (b) lasing. The bright bead-like scatterings are due to grating irregularities grown-in in a conventional substrate-grating DFB laser.

Fig. 12.   A [200] dark-field TEM photograph of the cross-sectional view of a 6-QW $In_{0.6}Ga_{0.4}As$(5 nm)/ $Q_{1.25}$(18.6 nm) active-layer DFB laser with a 2-QW $In_{0.62}Ga_{0.38}As$(4 nm)InP(9.3 nm) grating.

modify the coupling coefficient of the TE and TM modes of the DFB lasers. 7) If desired, a superlattice can be used in the grating instead of QW's. 8) Such QW grating can also be located on top of the active layers.

Therefore, it is seen that the introduction of QW (or superlattice) grating in DFB (or DBR) lasers will greatly facilitate the reproducible regrowth over grating and the control of the coupling coefficient. It will also provide a very convenient and effective scheme of achieving gain-coupled DFB lasers.

Figure 12 shows a transmission electron microscope photograph (the cross-sectional view) of a 6-QW active-layer DFB laser with a 2-QW grating. The fuzzy outline of the InP/InP grating interface is due to the nonexact perpendicular orientation of the sample with respect to the incident electron beam during viewing and the round uneven etched grating surface. Nevertheless, it is seen that the regrowth is defect free. It is also seen that the InP spacer layer smooths out the surface corrugation quickly compared with growth of quaternary over InP gratings.

To demonstrate that indeed these QW-grating DFB lasers have high-quality grating overgrowth, we studied the electroluminescence from window stripe lasers. In one conventional version of DFB lasers, the grating is fabricated onto the InP substrate surface, followed by overgrowth of a quaternary layer to produce the optical grating. Grating irregularities, originating from imperfections in the grating fabrication compounded

by a nonideal overgrowth of the quaternary waveguide layer, is known to produce strong light-scattering centers during lasing operation [30] as shown in Fig. 13(a) for a laser biased below threshold (10 mA) and above threshold (33 mA), Fig. 13(b). These light-scattering centers can be observed through a specially prepared top or bottom window parallel to the active stripe under a microscope equipped with an infrared video camera. They appear as irregular bright beads along the active stripe. The existence of such grating interfacial defects has a profound effect on device reliability, especially if they are strong strain centers. Dislocation generation at the grating interface during a device purging test has been recently reported [31]. Therefore improving grating interface becomes an important issue in all DFB-lasers. On the other hand, the present quantum well or superlattice gratings seem to eliminate the grating irregularity totally. The uniform thickness of the quantum wells eliminates the difficulty in grating amplitude control, while the grating overgrowth is facilitated by the growth of InP instead of a quaternary waveguide layer. Figure 14 shows electroluminescence and lasing images of the active stripe taken through a backside window prepared by carefully lapping the backside of the laser chip debonded from the laser mount. The images in Fig. 14(a) and 14(b) were taken at operation currents ($<$ 1 mA) below I_{th} and (65 mA) well above I_{th}, where the scattered laser light from the facets appears at each end of the active stripe, respectively. Under both operation conditions, the active stripe is uniformly bright and no light-scattering centers due to grating irregularities are observed, indicating that a much higher-quality grating overgrowth can be achieved by quantum wells compared to the conventional substrate-gratings.

To fabricate this, a uniform stack of n-type InGaAs/InP QW (or superlattice) of the desired number, composition, and thickness having a thin InP cap layer for grating fabrication was grown first over a 2-inch-diameter (100)-oriented n-InP substrate. We have fabricated such DFB laser wafers with the number of grating QW's varied from one to eight. For wafers with a large number of QW's, thinner QW's and InP barriers were used in order to maintain the total thickness $\lesssim$50 nm. In these cases, they behave more as superlattices than independent QW gratings. In the example shown by the TEM photograph in Fig. 12, two $In_{0.62}Ga_{0.35}As$ (slightly In-
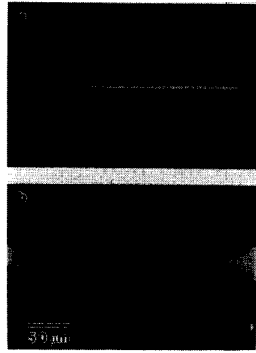
Fig. 14. The electroluminescence patterns along the laser stripe viewed through a contact window on the InP substrate when the 2-QW grating DFB laser is biased below (a) and above (b) lasing.
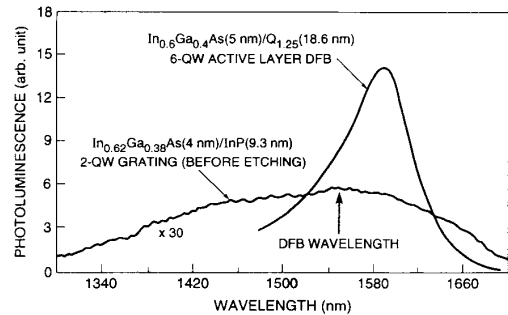

Fig. 15. The photoluminescence spectra from the two grating QW's before grating etching, and from the 6-QW active-layer DFB laser wafer after regrowth over the grating. The optical absorption by the 2-QW grating has extended well beyond the intended DFB lasing wavelength at 1.55 μm.
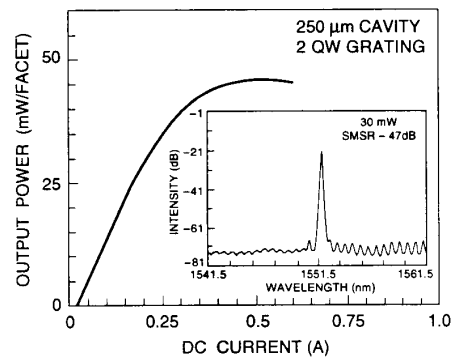

Fig. 16. The light–current characteristic of a typical 500-μm long laser with both facets AR-coated ($\sim$5%). The inset shows the lasing spectrum at $\sim$30 mW.

richer than the $In_{0.6}Ga_{0.4}As$ active QW's) QW's of 4 nm and InP barrier of 9.3 nm were grown. The top InP cap layer was 9.3 nm. First order gratings were prepared by standard holographic techniques and wet etching and had an amplitude of $\sim$48 nm, as shown in Fig. 12. No precise grating depth control was exercised here as long as the QW's were completely etched through. After cleaning, the sample was reintroduced into the CBE system for MQW laser regrowth. The detailed shape of the grating was well preserved, as shown by the TEM photograph. An n-type InP spacer layer of the desired thickness (65 nm in the present laser) was grown. The thickness of this layer will also affect the value of κ. This was then followed by the standard strained-layer 6-QW separate confinement heterostructure (SCH). The quaternary, $Q_{1.25}$, waveguide layers were 52.2 nm each. The $In_{0.6}Ga_{0.4}As$ QW's and $Q_{1.25}$ barriers were 5 nm and 18.6 nm, respectively. These laser wafers were further processed into buried heterostructure employing MOVPE regrowth of Fe-doped InP at 630 °C.

In this study we report the results obtained from a wafer with 2-QW $In_{0.62}Ga_{0.38}As$ grating (sample shown in Fig. 12). In this particular wafer, because the gain peak is located sufficiently (38 nm) longer in wavelength (see Fig. 15) than the DFB peak designed at 1550 nm, antireflection (AR) facet coatings ($\sim$5% on both facets) were employed to push the gain-peak towards the shorter wavelength. When the gain-peak was located closer to the DFB peak in the other wafers, even as-cleaved lasers show high side-mode suppression ratios (SMSR). However, we choose to present the results from this particular wafer because the total thickness of the two QW's was only 8 nm, and they were of $In_{0.62}Ga_{0.38}As$ material. This combination serves well to demonstrate the present proposed idea. The photoluminescence (PL) spectrum of this grating–QW structure was measured before grating etching and is shown in Fig. 15 together with the PL spectrum from the 6-QW $In_{0.6}Ga_{0.4}As$(5 nm)/$Q_{1.25}$(18.6 nm) active-layer DFB laser wafer after regrowth over the 2-QW grating. It is seen that optical absorption has extended well beyond 1550 nm. This suggests that the present QW grating will also produce a significant gain- (loss)-coupled component. The intensity is weak and broad because of doping and because the top InP capping layer is only 9.3 nm.

In Fig. 16 we show the L–I characteristic of a typical 500-μm-long laser. Output power of 46 mW/facet was obtained with a slope efficiency of $\sim$0.2 mW/mA/facet. The inset shows the lasing spectrum at $\sim$30 mW output. A SMSR of 47 dB was obtained. It is important to point out that even though the $In_{0.62}Ga_{0.38}As$ QW grating may introduce some additional loss, we have not observed unacceptable increases in threshold currents. For example, in the present case, the CW threshold currents were 13–18 mA even when the cavity length was 500 μm and both facets AR-coated, with the DFB mode far away from the gain peak. Figure 17 shows the SMSR as a function of injection current. A SMSR of $\sim$45 dB was maintained throughout the entire current range once lasing started. The inset shows the actual spectra up to 500 mA. Near threshold the DFB mode is relatively well centered, with a small Bragg stop-band. This indicates that the κ is small and a gain-coupled component is present.

The linewidths of 250-μm and uncoated lasers were also measured as a function of output power. Linewidth $\times$ power products of 1.9 to 4.0 were measured with minimum linewidths of 1.8-2.2 MHz. Fig. 18 shows the optical spectra at threshold (12 mA) without modulation and under 2.5 Gb/s modulation (32 mA). No detectable chirp was measured on the optical spectrum analyzer, which has a resolution of 0.1 nm. Mode partition characteristics at 2.5 Gb/s were measured with DC
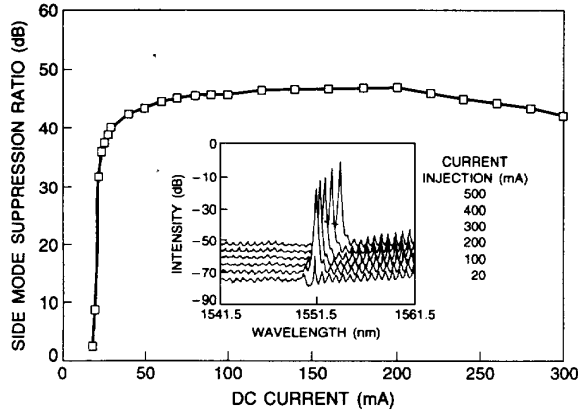
Fig. 17. The SMSR as a function of injection current. The inset shows the spectra at different injection currents. Near threshold the DFB mode is relatively well centered with a small Bragg stop-band.
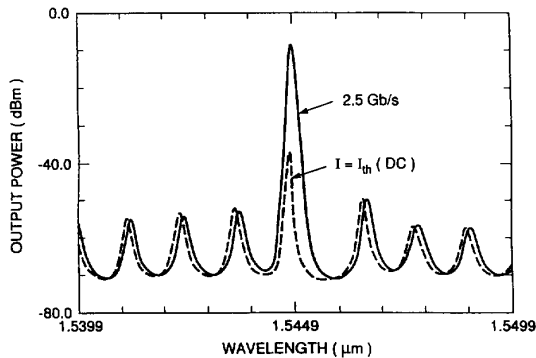

Fig. 18. The optical spectra at threshold with modulation and under 2.5 Gb/s modulation. No detectable chirp was measured. The optical spectrum analyzer has a resolution of 0.1 nm.

biased at $0.8\,I_{th}$, $0.9\,I_{th}$ and $1.0\,I_{th}$. It is seen that mode partition events shut off sharply as bias approaches I_{th} ($\gtrsim 0.95\,I_{th}$). Such behavior is very different from index-coupled DFB lasers, in which the mode partition events decrease slowly even when biased above threshold. Transmission experiments were carried out using such lasers as sources at 1.7 Gb/s over an amplified fiber system of 239 km. A very small dispersion penalty of 1.0 dB was measured at 10^{-11} BER. Such small dispersion penalties are among the lowest observed with DBR lasers and index-coupled DFB lasers. We would like to emphasize here that the above laser performance clearly demonstrates that these gain-coupled lasers are free of self-pulsation.

V. GAIN-SWITCHED DFB LASERS WITH QUANTUM- WELL LOSS GRATINGS

The generation of single-mode short optical pulses by semiconductor distributed-feedback (DFB) laser with near transform-limited bandwidth product at infrared wavelength is very important for many applications in fiber communication systems. Commonly used index-coupled semiconductor distributed feedback lasers have problems yielding single
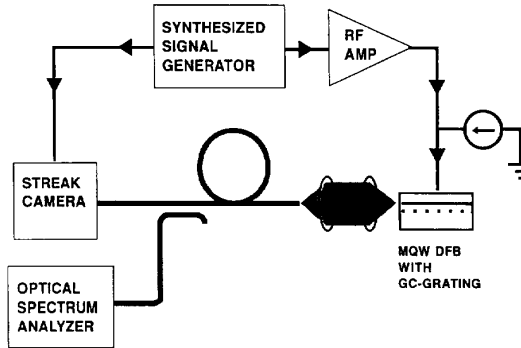

Fig. 19. The schematic diagram of test setups to measure the gain-switched lasers.

DFB mode because of the uncertainty of gratings-to-facet phases [11]. Short optical pulses have also been generated by gain-coupled DFB lasers with low wavelength chirping [31]. Here, we investigated the gain-switching behavior of the gain-coupled DFB lasers with quantum-well loss gratings.

The schematic diagram of the test setup is shown in Fig. 19. A synchro-scan streak camera was used to record the time domain optical pulses, while the time-average spectra were monitored by an optical spectrum analyzer. Without microwave modulation, this gain-coupled DFB laser is lasing at single mode with a side-mode suppression ratio greater than 40 dB. Because the amount of absorption in the QW gratings can be controlled by the indium composition of the QW's as well as the thickness of the InP spacer layer and QW's, no self-pulsation were observed over the whole dc bias regime. This had been verified by sending the optical signal into a high-speed detector mounted at the input of a highly sensitive microwave spectrum analyzer.

Fig. 20(a) shows the time trace recorded by steak camera. The laser was biased at 60 mA ($4 \times I_{th}$) and was driven by a microwave source at 4 GHz. It shows a 100% optical modulation depth with a FWHM pulse width of 23 ps. The average output power is 6.7 mW, and the peak power of the optical pulse is ~ 72 mW. The corresponding time-average spectrum is recorded in Fig. 20(b). The optical spectrum shows a FWHM bandwidth of 0.14 nm, which corresponds to a time-bandwidth product of 0.405. This is very close to the transform-limited value of 0.31 for a hyperbolic secant pulse shape or 0.44 for a Gaussian shape.

VI. DISTRIBUTED BRAGG REFLECTOR LASERS

Tunable distributed Braff reflector (DBR) lasers [32]–[34] are key elements for both a coherent and an incoherent wavelength-division-multiplexed (WDM) communication system. The DBR laser can be used as a transmitter, a local oscillator [35], and even an active filter [36]. Recently, it has also been considered as an ideal laser source for amplitude-shift-keying (ASK) transmission [37] due to its high side-mode suppression ratio (SMSR). In order to increase the threshold gain difference between the main mode and side modes of a DBR laser, we can 1) reduce the Bragg reflection bandwidth of the laser by using a weak and long waveguide grating and

TEMPORAL WAVEFORM   OPTICAL SPECTRUM
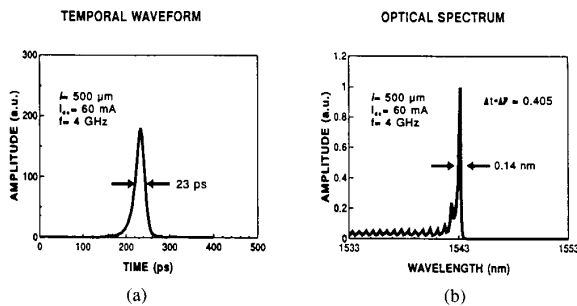

(a)   (b)

Fig. 20.   (a) Measured streak camera trace of a gain-coupled DFB laser with MQW loss gratings. The laser is driven by a 4-GHz microwave oscillator, and the pulse width is 23 ps. (b) The measured time-averaged spectrum corresponding to Fig. 3(a). The FWHM bandwidth of 0.14 nm corresponds to a time-bandwidth product of 0.405.
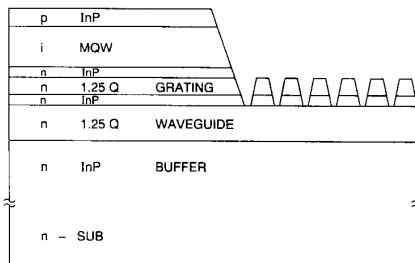

Fig. 21.   The growth layer structure of the DBR laser.

2) increase the longitudinal mode spacing by reducing the equivalent cavity length. In either case, the key parameter that needs to be well controlled is the grating coupling constant, κ. Taking the growth advantages of uniformity and well-controlled thickness by CBE, we fabricated DBR lasers with a record high SMSR of 58.5 dB.

The growth layer structure of the DBR laser is shown in Fig. 21. After a 600-nm thick InP buffer layer growth, a 1.25-μm wavelength InGaAsP, $Q_{1.25}$, waveguide layer with 270 nm thickness is grown. Followed by a thin InP etch stop layer, a 25-nm-thick $Q_{1.25}$ grating layer, and another InP etch-stop layer were grown. The multiquantum-well gain medium composed of six 5-nm-thick InGaAs strained quantum wells and six 12-nm $Q_{1.25}$ barriers. Finally, a p-type InP protection layer is grown as the top layer.

The grown wafer is processed by wet etching technique to remove the gain medium in the passive side. A holographic grating pattern is then generated and transferred to the grating layer through selective etching. Because the thickness of the grating layer is well controlled by the CBE growth time, the grating coupling constant, κ is also well defined. Followed by stripe etching and semi-insulating and p-cap layer regrowths, the wafer is further processed for multielectrode metalization. The lasers are cleaved with a gain section around 225 μm long and a grating section around 360 μm long.

The fabricated lasers have thresholds around 20 mA. The tuning range is 2.1 nm. The short tuning range may partly be caused by reduction of current tuning effect due to the "counter wavelength shift" by heat generation in such a long grating section. However, we have had no problem tuning
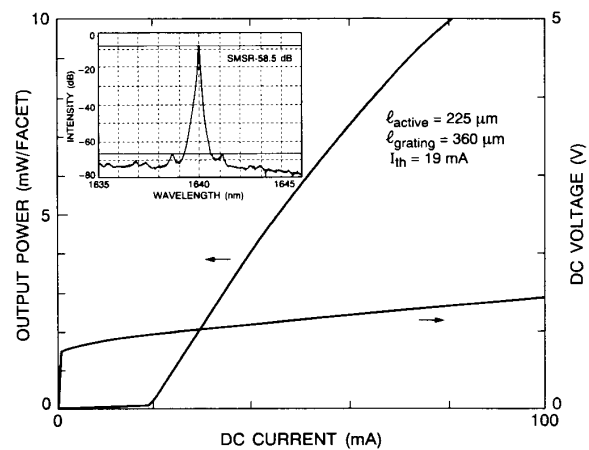

Fig. 22. L –I and I– V curves of one of the DBR lasers; the upper-left corner shows the output spectrum of the laser at 87 mA bias.

each laser to its Bragg-band center to obtain better mode behavior. Figure 22 shows the CW biased light–current curve and current–voltage curve of a laser and its SMSR at the bias of 87 mA. A record high SMSR of 58.5 dB has been achieved with these lasers. For most of the lasers, 10 mW output can be easily achieved and the measured output linewidths are below 10 MHz, which are attributed to the effect of the narrow Bragg bandwidth produced by the long and weak waveguide grating. The theoretically calculated κ of the layer structure employing the effective index method is around 50 cm^{-1}. Figure 23 shows the calculated and measured below-threshold noise spectra of a DBR laser with the gain and grating sections of 225 and 360 μm length, respectively. The waveguide loss we used in the calculation is 10 cm^{-1} for the passive guide, and 40 cm^{-1} for the active guide. As shown in both the theoretical and measured below-threshold spectra, the two side modes cannot grow with the increasing of bias, and the Bragg band is so narrow that only one mode is allowed inside the band.

VII. SUMMARY

In summary, we have demonstrated successful operation of long-wavelength InGaAsP low threshold-current index-coupled and gain-coupled DFB lasers. For index-coupled DFB lasers, buried-heterostructure six-QW DFB lasers (250 μm long and as-cleaved) operated at 1.55 μm with CW threshold currents of 10–15 mA and slope efficiencies up to 0.35 mW/mA (both facets). SMSR as high as 49 dB was obtained. The laser operated in the same DFB mode with SMSR staying above 40 dB from threshold and throughout the entire current range even at high temperatures (70 °C checked).

For gain-coupled DFB lasers, gain-coupling is accomplished by using an InGaAsP quaternary grating or quantum-well grating that absorbs the DFB emission. The use of a quantum-well grating, in particular, greatly facilitates reproducible regrowth (defect-free) over the grating and also control of the coupling coefficient. CW threshold currents were in the range of 10–15 mA for 250-μm and 13–18 mA for 250-μm and
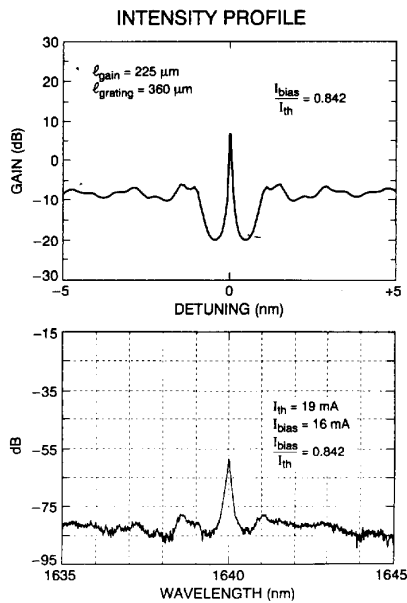
Fig. 23. Output noise spectra: upper, calculated; and lower, measured, of a DBR laser with 225- μm-long gain section and 360-μm-long grating section.

500- μm cavities, respectively. Slope efficiencies were high, $\sim$0.4 mW/mA (both facets). SMSR was as high as 52 dB and remained in the same DFB mode with SMSR staying $\sim$50 dB throughout the entire current range. Linewidth times power products of 1.9–4.0 were measured with minimum linewidths of 1.8–2.2 MHz. No detectable chirp was measured under 2.5 Gb/s modulation. Unlike index-coupled DFB lasers in which mode partition events decrease slowly even when biased above threshold, these lasers have mode partition events shut off sharply as bias approaches threshold ($\gtrsim$0.95 I_{th}). A very small dispersion penalty of 1.0 dB was measured at 10^{-11} BER in transmission experiments using these lasers as sources at 1.7 Gb/s over an amplified fiber system of 230 km. No self-pulsation was observed in these gain-coupled DFB lasers.

Gain-switching at 4 GHz with a 100% optical modulation depth and a FWHM pulse width of 23 ps was achieved with these gain-coupled DFB lasers. The peak power was $\approx$72 mW, and the FWHM bandwidth was 0.14 nm.

We also fabricated InGaAs/InGaAsP multiquantum-well DBR lasers by CBE. Taking advantage of uniform thickness growth and proper design of weak and long gratings, a record high SMSR of 58.5 dB was obtained.

REFERENCES

[1] Y. Suematsu, "Crystal growth, new structures and integration," 12th International Semiconductor Laser Conference, September 1990, Davos, Switzerland, Paper A1.

[2] T. Tanbun-Ek, R. A. Logan, S. N. G. Chu, A. M. Sergent, and K. W. Wecht, "Effects of strain in multiple quantum well distributed feedback lasers," Appl. Phys. Lett., vol. 57, pp. 2184–2186, 1990.

[3] P. J. A. Thijs, E. A. Monti, and T. van Dongen, "Structures for improved 1.5 μm wavelength lasers grown by LP-OMVPE InGaAsP/InP strained-layer quantum wells a good candidate," J. Cryst. Growth, vol. 107, pp. 731–740, 1991.

[4] W. T. Tsang, "Progress in chemical beam epitaxy," J. Crystal Growth, vol. 105, pp. 1–29, 1990.

[5] W. T. Tsang, F. S. Choa, M. C. Wu, Y. K. Chen, A. M. Sergent, and P. F. Sciortino, Jr., "Very low threshold single quantum well graded-index separated confinement heterostructure InGaAs/InGaAsP lasers grown by chemical beam epitaxy," Appl. Phys. Lett., vol. 58, pp. 2610–2612, 1991.

[6] T. L. Koch, P. J. Corvini, U. Koren, and W. T. Tsang, "Wavelength uniformity of 1.3 μm GaInAsP/InP distributed-Bragg-reflector lasers with hybrid beam/vapour epitaxial growth," Electron. Lett., vol. 24, pp. 822–824, 1988.

[7] W. T. Tsang, M. C. Wu, T. Tanbun-Ek, R. A. Logan, S. N. G. Chu, and A. M. Sergent, "Low threshold and high power output 1.5 μm InGaAs/InGaAsP separate confinement multiple quantum well laser grown by chemical beam epitaxy," Appl. Phys. Lett., vol. 57, pp. 2065–2067, 1990.

[8] H. Heinecke, B. Baur, N. Emeis, and M. Schier, "Growth of high purity InP by CBE," J. Cryst. Growth, vol. 105, pp. 143–148, 1990.

[9] A. Takemoto, Y. Okhura, H. Watanabe, Y. Nakajima, Y. Sakakibara, S. Kakimoto, and H. Namizaki, "Dependence of characteristics of buried grating type DFB laser diodes on coupling constant," 12th International Semiconductor Laser Conf., September 1990, Davos, Switzerland, Paper E-3.

[10] W. T. Tsang, F. S. Choa, M. C. Wu, Y. K. Chen, R. A. Logan, T. Tanbun-Ek, S. N. G. Chu, K. Tai, A. M. Sergent, and K. W. Wecht, "1.5 μm wavelength InGaAs/InGaAsP distributed feedback multi-quantum-well lasers grown by chemical beam epitaxy," Appl. Phys. Lett., vol. 59, pp. 2375–2377, 1991.

[11] J. Buss, "Mode selectivity in DFB lasers with cleaved facets," Electron. Lett., vol. 21, pp. 179–180, 1985.

[12] J. Kinoshita and K. Matsumoto, "Yield analysis of SML DFB lasers with an axially-flattened internal field," IEEE J. Quantum Electron., vol. 25, pp. 1324–1332, 1989.

[13] H. Soda, Y. Kotaki, H. Sudo, H. Ishikawa, S. Yamakoshi, and H. Imai, "Stability in single longitudinal mode operation in GaInAsP/InP phase-adjusted DFB lasers," IEEE J. Quantum Electron., vol. 23, pp. 804–814, 1987.

[14] K. David, G. Morthier, P. Vankwikelberge, R. G. Baets, T. Wolf, and B. Borchert, "Gain-coupled DFB lasers versus index-coupled and phase-shifted DFB lasers: A comparison based on spatial hole burning corrected yield," IEEE J. Quantum Electron., vol. 27, pp. 1714–1724, 1991.

[15] H. Kogelnik and C. V. Shank, "Coupled-wave theory of DFB lasers," J. Appl. Phys., vol. 43, pp. 2327–2335, 1972.

[16] M. Okai, T. Tsuchiya, K. Uomi, N. Chinone, and T. Harada, "Corrugation-pitch modulated MQW-DFB lasers with narrow spectral width," IEEE J. Quantum Electron., vol. 27, pp. 1767–1772, 1991.

[17] Y. Luo, Y. Nakano, K. Tada, T. Inoue, H. Hosomatsu, and H. Iwaoka, "Fabrication and characteristics of gain-coupled DFB lasers with a corrugated active layer," IEEE J. Quantum Electron., vol. 27, pp. 1724–1731, 1991.

[18] {—}{—}, "Purely gain-coupled DFB Laser," Appl. Phys. Lett., vol. 56, pp. 1620–1622, 1990.

[19] E. Kapon, A. Hardy, and A. Katzir, "The effects of complex coupling coefficients on DFB lasers," IEEE J. Quantum Electron., vol. 18, pp. 66–71, 1982.

[20] G. Morthier, P. Vankwikelberge, K. David, and R. Baets, "Improved performance of AR-coated DFB lasers by the introduction of gain-coupling," IEEE Photon. Technol. Lett., vol. 2, pp. 170–172, 1990.

[21] K. David, G. Morthier, P. Vankwikelberge, and R. Baets, "Yield analysis of non-AR-coated DFB lasers with combined index and gain coupling," Electron. Lett., vol. 26, pp. 238–239, 1990.

[22] Y. Nakano, Y. Luo, and K. Tada, "Facet reflection independent, single longitudinal mode oscillation in a GaAlAs/GaAs DFB laser equipped with gain-coupling mechanism," Appl. Phys. Lett., vol. 55, pp. 1606–1608, 1989.

[23] Y. Nakano, Y. Deguchi, K. Ikeda, Y. Luo, and K. Tada, "Reduction of excess intensity noise induced by external reflection in a gain-coupled DFB laser," IEEE J. Quantum Electron., vol. 27, pp. 1732–1735, 1991.

[24] T. Inoue, S. Nakajima, T. Oki, H. Iwaoka, Y. Nakano, and K. Tada, "High-performance InGaAsP/InP Gain-coupled DFB laser," presented at 17th European Conf. Opt. Comm., Paris, France, 1991, post-deadline paper 5.

[25] B. Borchert, K. David, B. Stegmuller, R. Gessner, M. Beschorner, D. Sacher, and G. Franz, "1.55 μm gain-coupled quantum well DFB with high single-mode yield and narrow linewidth," IEEE Photon. Technol. Lett., vol. 3, pp. 953–955, 1991.

[26] W. T. Tsang, F. S. Choa, R. A. Logan, T. Tanbun-Ek, and A. M. Sergent, "All-gaseous doping during chemical beam epitaxial growth of InGaAs/InGaAsP multi-quantum well lasers," Appl. Phys. Lett., vol. 59, pp. 1008–1010, 1991.

[27] W. T. Tsang, F. S. Choa, M. C. Wu, Y. K. Chen, R. A. Logan, T. Tanbun-Ek, S. N. G. Chu, K. Tai, A. M. Sergent, and K. W. Wecht, "1.5 μm wavelength InGaAs/InGaAsP distributed feedback multiquantum well lasers grown by chemical beam epitaxy," *Appl. Phys. Lett.*, vol. 59, pp. 2375–2377, 1991.
[28] W. T. Tsang, N. A. Olsson, and R. A. Logan, "Threshold-wavelength and threshold-temperature dependences of GaInAsP/InP lasers with frequency selective feedback operating in the 1.3- and 1.5-μm regions," *Appl. Phys. Lett.*, vol. 43, pp. 154–156, 1983.
[29] E. J. Flynn (unpublished).
[30] S. N. G. Chu and S. Nakahara, "Cross-sectional transmission electron microscopy parallel to the active stripe of degraded buried heterostructure distributed feedback laser devices," *Appl. Phys. Lett.*, vol. 62, pp. 917–919, 1993.
[31] Y. Luo, R. Takahashi, Y. Nakano, K. Tada, T. Kamiya, H. Hosomatsu, and H. Iwaoka, "Ultralow chirping short optical pulse (16 ps) generation in gain-coupled DFB lasers," *Appl. Phys. Lett.*, vol. 59, p. 37, 1991.
[32] Y. Kotaki, M. Matsuda, M. Yano, H. Ishkawa, and H. Imai, "1.55 μm wavelength tunable FBH-DBR laser," *Electron. Lett.*, vol. 23, p. 327, 1987.
[33] S. Murata, I. Mito, and K. Kobayashi, "Over 720 GHz (5.8 nm) frequency tuning by a 1.5 μm DBR laser with phase and Bragg wavelength control regions," *Electron. Lett.*, vol. 23, p. 405, 1987.
[34] T. L. Koch, U. Koren, R. P. Gnall, C. A. Burrus, and B. I. Miller, "Continuously tunable 1.5 μm multiple-quantum-well GaInAs/GaInAsP distributed-Bragg-reflector lasers," *Electron. Lett.*, vol. 24, p. 1431, 1988.
[35] T. L. Koch, U. Koren, R. P. Gnall, F. S. Choa, F. Hernandez-Gil, C. A. Burrus, M. G. Young, M. Oron, and B. I. Miller, "GaInAs/GaInAsP multiple-quantum-well integrated heterodyne receiver," *Electron. Lett.*, vol. 25, p. 1621, 1989.
[36] T. L. Koch, F. S. Choa, F. Heismann, and U. Koren, "Tunable multiple-quantum-well distributed-Bragg-reflector lasers as tunable narrowband receivers," *Electron. Lett.*, vol. 25, p. 890, 1989.
[37] K. C. Reichmann, P. D. Magill, S. L. Woodward, U. Koren, T. L. Koch, and B. I. Miller, "Directly modulated DBR lasers for long-haul transmission at 1.7 Gbit/s," Tech. Digest OFC'92, 1992, paper TuD6, p. 26.

W. T. Tsang (M'84–SM'89–F'90), photograph and biography not available at the time of publication.

M. C. Wu, photograph and biography not available at the time of publication.

Y. K. Chen photograph and biography not available at the time of publication.

F. S. Choa (S'85–M'88), photograph and biography not available at the time of publication.

R. A. Logan (M'73–SM'73–F'86), photograph and biography not available at the time of publication.

S. N. G. Chu, photograph and biography not available at the time of publication.

A. M. Sergent, photograph and biography not available at the time of publication.

P. Magill, photograph and biography not available at the time of publication.

K. C. Reichmann, photograph and biography not available at the time of publication.

C. A. Burrus (SM'63–F'74), photograph and biography not available at the time of publication.